Optics Letters

Observation of a comb of squeezed states with a strong squeezing factor by a bichromatic local oscillator

Shaoping Shi,[1] Yajun Wang,[1,2] Long Tian,[1,2] Jinrong Wang,[1] Xiaocong Sun,[1] and Yaohui Zheng[1,2,*]

[1]State Key Laboratory of Quantum Optics and Quantum Optics Devices, Institute of Opto-Electronics, Shanxi University, Taiyuan 030006, China
[2]Collaborative Innovation Center of Extreme Optics, Shanxi University, Taiyuan, Shanxi 030006, China
*Corresponding author: yhzheng@sxu.edu.cn

Received 16 December 2019; revised 15 February 2020; accepted 17 March 2020; posted 17 March 2020 (Doc. ID 385912); published 15 April 2020

We demonstrate the experimental detection of an optical squeezing covering several higher resonances of the optical parametric amplifier (OPA) by adopting a bichromatic local oscillator (BLO). The BLO is generated from a waveguide electro-optic phase modulator (WGM) and subsequent optical mode cleaner (OMC), without the need of additional power balance and phase control. The WGM is used for generating the frequency-shifted sideband beams with equal power and certain phase difference, and the OMC is used for filtering the unwanted optical modes. Among a measurement frequency range from 0 to 16.64 GHz, the maximum squeezing factors are superior to 10 dB below the shot noise limit for the first three discrete odd-order resonances of the OPA.

https://doi.org/10.1364/OL.385912

Squeezed states, with fewer fluctuations in one quadrature than vacuum noise at the expense of increased fluctuations in the other quadrature [1–3], play an important role in gravitational wave (GW) detection [4–7] and quantum information technology [8,9]. To improve the performance of these applications as much as possible, it is extremely important to have the ability to detect a squeezed state with a strong squeezing factor [10–12]. Another point to consider is that its frequency band should be compatible with the practical application. Since the Laser Interferometer Gravitational-Wave Observatory (LIGO) locates in the 10 Hz to 10 kHz band, squeezing in the audio band has been demonstrated [6,7,13,14]. For the application of quantum communication, the data rate is dependent not only the squeezing strength, but also the squeezing bandwidth, driving the bandwidth extension to gigahertz (GHz) level by designing an optical parametric amplifier (OPA) with large bandwidth [15–17]. On this basis, channel multiplexing can further multiply the data rate of quantum communication [18]. Irrespective of the details of the coding protocol, a multiplexing scheme must allow all users to have access to a high-capacity channel without experiencing interference from each other, in analogy with frequency comb shape [19]. In the quantum communication system, the data rate for a comb of squeezing spectrum is always greater than that for a white squeezing one [18]. Squeezed states can be described as the beats between pairs of quantum correlated upper and lower sidebands around half the pump beam frequency. All these downconversion modes are subject to energy conservation and cavity resonance condition within the phase-matching bandwidth of nonlinear crystal, which present quantum correlations with a noise power spectrum like a frequency comb [20].

Balanced homodyne detection (BHD), which extracts the quadrature information from an optical field, is a cornerstone method for quantum optics [21,22]. A comb of optical squeezing was detected over 5.1 GHz bandwidth by adopting two different detectors, one for low-frequency detection, and another for high-frequency detection [23]. However, the detector's clearance between the electronics noise and shot noise above 1.5 GHz is approximately 3 dB, which is impossible to directly detect strong squeezing. Therefore, the upper limit of the detection frequency is inherently limited by the electronic bandwidth of the BHD, not the generation process [24]. Limited by the dark noise of the BHD, it was impossible to direct detect a strong squeezing with such a broadband BHD. Heterodyne detection using a bichromatic local oscillator (BLO), frequency shifted near the detection frequency, can eliminate the above limitation and allow low-noise detection at arbitrarily high frequency [25–27]. Li *et al.* demonstrated squeezed state detection at low-frequency band with the squeezing factor of 4.1 dB, by using a BLO. The BLO has a frequency shift of ±5 MHz generated from three acousto-optic modulators (AOMs) [28]. A pair of local oscillators (LOs) serving as the BLO was carefully controlled to balance their power and stabilize their relative phase. The scheme that generates a pair of LOs becomes more complex and expensive as the frequency difference is increased. In principle, a BLO can be also generated from electro-optic modulators (EOMs) [29,30]. The upper and lower sidebands of the EOM have the same power and certain phase relationship, which meet the requirement for BLO, and this method is a simpler scheme for BLO generation.

In this Letter, we demonstrate the experimental measurements of the squeezing and antisqueezing levels for the first three odd-order resonances of OPA from 0 to 16.64 GHz by means of several pairs of frequency-shifted LOs. The maximum noise variances for each resonance over the measurement frequency range are superior to 10 dB below the shot noise limit (SNL). Our balanced detector (BD) covers an electronic bandwidth of 100 MHz, which can satisfy the detection demand for the squeezing factor within the linewidth of each resonance of the OPA. The BLO extends the measurement frequency to higher-order resonance, dependent of the amount of frequency shift. A pair of frequency-shifted LOs is generated by a waveguide electro-optic phase modulator (WGM) and subsequent specially designed optical mode cleaner (OMC) is used for filtering the unwanted optical modes. The scheme saves the tedious steps for the power balance and phase control between the two LOs. With the aid of a high-bandwidth WGM, we expect to directly detect strong squeezing at higher frequency without changing the experimental parameters.

A schematic of our experimental setup is illustrated in Fig. 1. The laser source is a continuous-wave single-frequency Nd:YVO_4 laser at 1064 nm with an output power of 2.5 W. The laser preparations, including spatial-mode improvement, polarization purification, and second-harmonic generation, are similar to our earlier experiments presented in Refs. [31–34]. The laser beam at 1064 nm serves as the initial alignment of OPA. The reference beam B1 is used for the stable control of the OPA length and relative phase, and the beam B2 is used for the generation of BLO. The phase modulated signal with the modulation frequency of 36 MHz is imprinted on the reference beam B1 by electro-optic modulator (EOM1) to extract error signals for controlling the OPA cavity length and relative phase between the pump and signal beams. Our OPA is a semimonolithic cavity consisting of a piezoactuated concave mirror and a PPKTP crystal with the dimensions of 1 mm × 2 mm × 10 mm. The crystal end face with a radius of curvature of 12 mm is coated as high reflectivity for the fundamental field, thus serving as the cavity end mirror. The concave mirror with a radius of curvature of 30 mm has a transmissivity of 12% ± 1.5% for 1064 nm. The air gap between the crystal and the coupling mirror is 26.8 mm, corresponding to a free spectral range (FSR) ω_f of 3.328 GHz. Here, the phase-matching bandwidth of the PPKTP crystal is

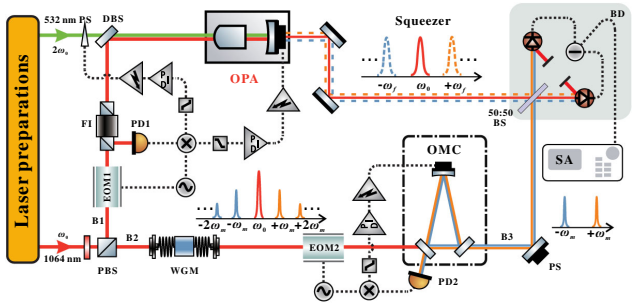

Fig. 1. Schematic of the experimental setup. OPA, optical parametric amplifier; WGM, waveguide electro-optic modulator; EOM, electro-optic phase modulator; OMC, optical mode cleaner; FI, Faraday isolator; PS, phase shifter; DBS, dichroic beam splitter; PBS, polarized beam splitter; BS, beam splitter; BD, balanced detector; PD, photodetector; PID, proportion integration differentiator; ω_f, free spectral range of the OPA; ω_m, modulation frequency ($\omega_m = k\omega_f$, k is odd number).

approximately 2 THz, corresponding to more than 300 pairs of downconversion modes subject to cavity resonance condition. The pump field at 532 nm does not resonate with the OPA, which has good immunity to temperature variation. The relative phase between the pump and signal beams is locked at the most deamplified phase π.

The beam B2 is coupled into a WGM to generate the upper and lower sideband beams, and the two symmetric sidebands along the carrier frequency have the same power and overlap with each other in space. For a WGM, the phase difference between these upper and lower sidebands is 0 (π). The positive and negative sidebands of the squeezed state also have a certain phase difference of π. When simultaneously scanning the phase of the BLO, we can measure the same quadrature component of the positive and negative sidebands without additional phase stability.

For a single modulation frequency ω_f, the output of the WGM includes the carrier ω_0, sideband frequency $\omega_0 \pm \omega_f$, and its higher harmonics $\omega_0 \pm n\omega_f$ (n is integer). We employ an OMC as an optical filter to reflect the unwanted optical modes and transmit odd-order sideband modes $\omega_0 \pm m\omega_f$ (m is odd number) for the BLO. The OMC consists of two plane mirrors and one curved mirror, and the curved cavity mirror shows a reflectivity of 99.997% with the curvature radius of 1.0 m. The round trip length is approximately 225.2 mm, which can be finely manipulated to make two first-order sideband modes $\omega_0 \pm \omega_f$ resonate simultaneously with the OMC. The carrier mode ω_0 is located between transmission peaks of the two sideband modes $\omega_0 \pm \omega_f$. The two plane cavity mirrors have a power transmissivity of 0.5% for the s-polarized beam, corresponding to the finesse value of 620 and linewidth of 2 MHz. The OMC has a power transmission of 80% for the resonant sideband. The transmission of the carrier mode ω_0 and even-order sideband modes $\omega_0 \pm 2n\omega_f$ is less than 0.001% when the OMC resonates with the sideband modes $\omega_0 \pm \omega_f$, meaning the suppression factor is about 10^{-5} for the carrier and unwanted sideband modes, which is enough to measure the correlation variance of the upper and lower sidebands near the sideband modes $\omega_0 \pm \omega_f$ without interference from neighboring resonance modes. In order to reduce the influence of a higher harmonics sideband on the measurement of correlation variance, such as $\omega_0 \pm 3\omega_f$, we impose a modulation index on the WGM as low as possible under the premise of ensuring enough power of the BLO. Here, the modulation depth is 0.5, the total power of first-order sideband modes $\omega_0 \pm \omega_f$ is 4 mW at the input power of 100 mW corresponding to the clearance between the shot noise and electronic noise of 29.2 dB. At this point, the influence of the electronic noise on the measured squeezed degree can be neglected. For the modulation depth of 0.5, the power of third-order sideband modes $\omega_0 \pm 3\omega_f$ is only 0.01% of that of first-order sideband modes $\omega_0 \pm \omega_f$, and the measurement error originating from the sideband modes $\omega_0 \pm 3\omega_f$ is less than 0.0004 dB. The OMC is held on resonance with two sideband modes $\omega_0 \pm \omega_f$ via a Pound–Drever–Hall technique [35]. For the measurement of the even-order sideband modes $\omega_0 \pm 2n\omega_f$, the length of the OMC is no longer as a constant, but dependent on the frequency difference of the measured two sideband modes, which should be considered to simultaneously suppress the carrier mode. With a fixed cavity length for a specially designed OMC, we can generate the BLO covering the frequency range of all odd-order sideband modes. Therefore, we

pay attention to the squeezing measurement of the odd-order sideband modes.

The squeezed light, emitting out from the OPA, is interfered with the BLO on a 50:50 beam splitter (BS). We achieve a fringe visibility of 99.8% between the signal beam and the carrier mode ω_0 of the beam B3, indicating a perfect mode overlap between the two detected sideband modes. After the BS, the output beams are coupled toward a BD to detect the noise variations. The detector is built from a pair of p-i-n photodiodes with the photo surface of 100 μm. We scan the phase of the BLO by a phase shifter located in the BLO path. To recycle the residual reflection from photodiode surfaces, two concave mirrors with the curvature radius of 50 mm are used as the retroreflectors.

Here, a signal beam with the power of 15 mW is injected into the OPA for the cavity and relative phase locking, and we measure the squeezing factor when the BLO operates at the sideband modes of $\omega_0 \pm \omega_f$. Figure 2 shows the observed squeezing levels at the analysis frequency of 9 kHz, with a resolution bandwidth (RBW) of 1 kHz and a video bandwidth (VBW) of 50 Hz, after all degrees of freedom are stably controlled. All traces are measured by a spectrum analyzer without the electronic noise subtracted (R&S FSW8). The SNL (Trace a) is recorded with the squeezed light blocked. Trace (b) is a noise level with the BLO phase scanned simultaneously. The directly observed correlation variance is 10.2 dB below the SNL. The nonclassical noise suppression cannot be observed at audio band by adopting the BHD. In terms of BHD, laser noise and technical noise from the locking loops near the carrier mode ω_0 are dominant and corrupt the correlation variance [13,23,33], which can be improved by a vacuum seeded optical parametric oscillator (OPO). The high-order sideband mode $\omega_0 \pm n\omega_f$ is immune to laser noise that is often present at audio band, even with a coherent seeded OPO.

Subsequently, we measure the noise variances at the first, third, and fifth resonance of the OPA by respectively employing three pairs of sideband modes $\omega_0 \pm \omega_f$, $\omega_0 \pm 3\omega_f$, and $\omega_0 \pm 5\omega_f$ as the BLO. If the WGM has a modulation bandwidth of 1 THz, we expect to detect the first 150 odd-order downconversion modes. The frequency switching of the BLO is conveniently implemented by changing the driving frequency of the WGM, without the need of any realignment and

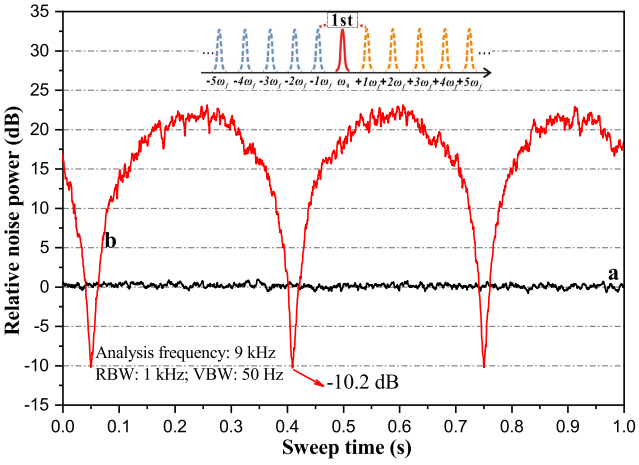

Fig. 2. Quantum noise variances are recorded at the analysis frequency of 9 kHz; the BLO is first-order sideband modes $\omega_0 \pm \omega_f$. RBW, resolution bandwidth; VBW, video bandwidth.

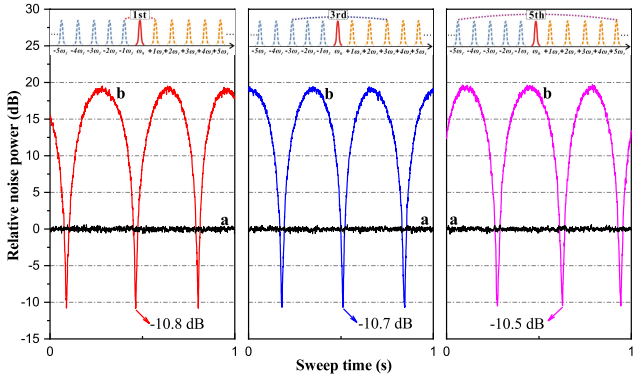

Fig. 3. Quantum noise levels of the squeezed and antisqueezed state as the LO phase is being scanned at the first, third, and fifth resonance of the OPA (3.328 GHz, 9.984 GHz, 16.64 GHz). These data still include electronic noise and represent direct observations.

broadband detector. The measurement results at the analysis frequency of 2 MHz, as shown in Fig. 3, are normalized with a RBW of 300 kHz and a VBW of 200 Hz. 10.8 dB squeezing at first resonance of the OPA (3.328 GHz), 10.7 dB squeezing at third resonance (9.984 GHz), and 10.5 dB squeezing at resonance (16.64 GHz) are respectively observed. Limited by the low clearance of the BHD at high-frequency band [16,17,23], it is impossible to directly detect a strong squeezing at high frequency up to several GHz. The BLO technique can compensate the frequency discrepancy between the sideband and carrier modes by shifting the frequency of the LO, which provide an approach for measurement of a strong squeezing at the high-frequency band. Owing to the large phase-matching bandwidth of the PPKTP, we have strong reason to believe that the discrepancy of the squeezing factor among several resonances of the OPA comes from the detection process, not the generation process.

Figure 4 presents the quadrature variance spectrum of bright squeezed light at the frequency range from 1 MHz to 70 MHz when the BLO operates at the sideband mode $\omega_0 \pm \omega_f$. 10.8 dB and 2.3 dB of squeezing at the analysis frequency of 1 MHz and 70 MHz are observed. The squeezing spectrum is well matched

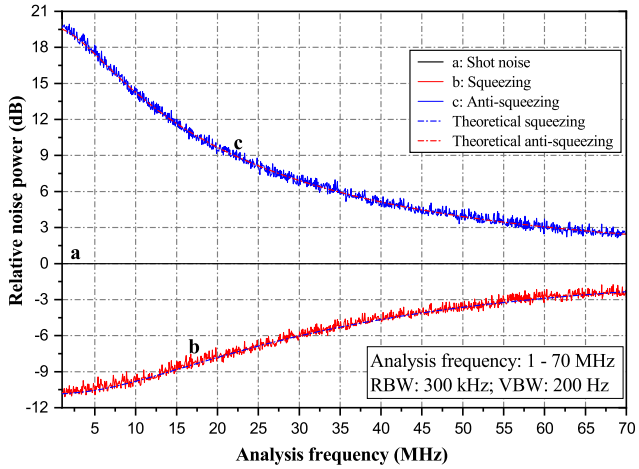

Fig. 4. Normalized quantum noise spectrum at the analysis frequency from 1 MHz to 70 MHz. RBW, resolution bandwidth; VBW, video bandwidth. The linewidth of the OPA is 68 MHz.

to the theoretical simulation by the quadrature variance expression presented in Refs. [31,36–38]. We do also obtain the similar results as Fig. 4 at the third- and fifth-order sideband modes, in which only the squeezing factor has tiny difference; hence, the figures are omitted.

In conclusion, we measured experimentally the squeezing and antisqueezing factors covering several resonances of the OPA by means of the BLO. A WGM and subsequent specially designed OMC are employed to generate the frequency-shifted BLO, the WGM is used for generating the frequency-shifted sideband modes, and the OMC is used for filtering the unwanted optical modes. The two symmetric sidebands have the same power and certain phase, which method simplifies greatly the generation process of the BLO. The noise variances at the first, third, and fifth resonance of the OPA are respectively quantified by employing three pairs of sideband modes $\omega_0 \pm \omega_f$, $\omega_0 \pm 3\omega_f$, and $\omega_0 \pm 5\omega_f$ as the BLO, without the need of broadband detector [16,17,23]. All the maximum squeezing factors for the three sideband modes are more than 10 dB. The squeezing bandwidth for each individual sideband mode is 68 MHz. Of course, the squeezing bandwidth of each individual sideband mode can be expanded to GHz level, shown in [16,17]. In combination with the BLO technique presented here, a comb of squeezed states that has GHz bandwidth of each individual sideband mode can be observed. The number of the detected resonance modes is limited by the modulation bandwidth of our WGM, not by the generation process. We expect to observe the squeezing to higher-order sideband modes by simply expanding the modulation bandwidth. It can help to save quantum resources and enhance the capacity of quantum channels to extent to a large scale practical quantum system.

Funding. National Natural Science Foundation of China (11654002, 11874250, 11804207, 11804206); National Key Research and Development Program of China (2016YFA0301401); Program for Sanjin Scholar of Shanxi; Fund for Shanxi "1331 Project" Key Subjects Construction; Program for Outstanding Innovative Teams of Higher Learning Institutions of Shanxi; Key Research and Development (R&D) Projects of Shanxi province (201903D111001).

Disclosures. The authors declare no conflicts of interest.

REFERENCES

1. D. F. Walls, Nature **306**, 141 (1983).
2. L. A. Wu, H. J. Kimble, J. L. Hall, and H. Wu, Phys. Rev. Lett. **57**, 2520 (1986).
3. G. Breitenbach, S. Schiller, and J. Mlynek, Nature **387**, 471 (1997).
4. K. Goda, O. Miyakawa, E. E. Mikhailov, S. Saraf, R. Adhikari, K. Mchenzie, R. Ward, S. Vass, A. J. Weinstein, and N. Mavalvala, Nat. Phys. **4**, 472 (2008).
5. H. Grote, K. Danzmann, K. L. Dooley, R. Schnabel, J. Slutsky, and H. Vahlbruch, Phys. Rev. Lett. **110**, 181101 (2013).
6. M. Tse, H. Yu, N. Kijbunchoo, A. Fernandez-Galiana, P. Dupej, L. Barsotti, C. D. Blair, D. D. Brown, S. E. Dwyer, A. Effler, and M. Evans, Phys. Rev. Lett. **123**, 231107 (2019).
7. Virgo Collaboration, Phys. Rev. Lett. **123**, 231108 (2019).
8. S. L. Braunstein and P. van. Loock, Rev. Mod. Phys. **77**, 513 (2005).
9. A. Furusawa, J. L. Sorensen, S. L. Braunstein, C. A. Fuchs, J. J. Kimble, and E. S. Polzik, Science **282**, 706 (1998).
10. H. Vahlbruch, M. Mehmet, K. Danzmann, and R. Schnabel, Phys. Rev. Lett. **117**, 110801 (2016).
11. M. Mehmet, S. Ast, T. Eberle, S. Steinlechner, H. Vahlbruch, and R. Schnabel, Opt. Express **19**, 25763 (2011).
12. X. C. Sun, Y. J. Wang, L. Tian, Y. H. Zheng, and K. C. Peng, Chin. Opt. Lett. **17**, 072701 (2019).
13. K. McKenzie, N. Grosse, W. P. Bowen, S. E. Whitcomb, M. B. Gray, D. E. McClelland, and P. K. Lam, Phys. Rev. Lett. **93**, 161105 (2004).
14. W. Li, Y. Jin, X. Yu, and J. Zhang, Phys. Rev. A **96**, 023808 (2017).
15. H. Yonezawa, S. L. Braunstein, and A. Furusawa, Phys. Rev. Lett. **99**, 110503 (2007).
16. S. Ast, A. Samblowski, M. Mehmet, S. Steinlechner, T. Eberle, and R. Schnabel, Opt. Lett. **37**, 2367 (2012).
17. S. Ast, M. Ast, M. Mehmet, and R. Schnabel, Opt. Lett. **41**, 5094 (2016).
18. M. Heurs, J. G. Webb, A. E. Dunlop, C. C. Harb, T. C. Ralph, and E. H. Huntington, Phys. Rev. A **81**, 032325 (2010).
19. B. Sklar, IEEE Signal Process. Mag. **20**, 87 (2003).
20. J. Roslund, R. Medeiros, S. F. Jiang, C. Fabre, and N. Treps, Nat. Photonics **8**, 109 (2014).
21. Y. Shaked, Y. Michael, R. Z. Vered, L. Bello, M. Rosenbluh, and A. Pe'er, Nat. Commun. **9**, 609(2018).
22. M. S. Stefszky, C. M. Mow-Lowry, S. S. Y. Chua, D. A. Shaddock, B. C. Buchler, H. Vahlbruch, A. Khalaidobski, R. Schnabel, P. K. Lam, and D. E. McClelland, Classical Quantum Gravity **29**, 145015 (2012).
23. R. J. Senior, G. N. Milford, J. Janousek, A. E. Dunlop, K. Wagner, H. A. Bachor, T. C. Ralph, E. H. Huntington, and C. C. Harb, Opt. Express **15**, 5310 (2007).
24. B. Hage, A. Samblowski, and R. Schnabel, Phys. Rev. A **81**, 062301 (2010).
25. A. M. Marino, J. C. R. Stroud, V. Wong, R. S. Bennink, and R. W. Boyd, J. Opt. Soc. Am. B **24**, 335 (2007).
26. C. S. Embrey, J. Hordell, P. G. Petrov, and V. Boyer, Opt. Express **24**, 27298 (2016).
27. S. Feng, D. He, and B. Xie, J. Opt. Soc. Am. B **33**, 1365 (2016).
28. W. Li, X. D. Yu, and J. Zhang, Opt. Lett. **40**, 5299 (2015).
29. M. Pysher, Y. Miwa, R. Shahrokhshahi, R. Bloomer, and O. Pfister, Phys. Rev. Lett. **107**, 030505 (2011).
30. B. Xie, P. Yang, and S. Feng, J. Opt. Soc. Am. B **35**, 2342 (2018).
31. W. H. Yang, S. P. Shi, Y. J. Wang, W. G. Ma, Y. H. Zheng, and K. C. Peng, Opt. Lett. **42**, 4553 (2017).
32. S. P. Shi, Y. J. Wang, W. H. Yang, Y. H. Zheng, and K. C. Peng, Opt. Lett. **43**, 5411 (2018).
33. X. C. Sun, Y. J. Wang, L. Tian, S. P. Shi, Y. H. Zheng, and K. C. Peng, Opt. Lett. **44**, 1789 (2019).
34. H. Y. Zhang, J. R. Wang, Q. H. Li, Y. J. Ji, Z. Y. He, R. C. Yang, and L. Tian, Acta Sin. Quantum Optica **25**, 456 (2019).
35. E. D. Black, Am. J. Phys. **69**, 79 (2001).
36. S. Dwyer, L. Barsotti, S. S. Y. Chua, M. Evans, M. Factourovich, D. Gustafson, T. Isogai, K. Kawabe, A. Khalaidovski, P. K. Lam, M. Landry, N. Mavalvala, D. E. McClelland, G. D. Meadors, C. M. Mow-Lowry, R. Schnabel, R. M. S. Schofield, N. Smith-Lefebvre, M. Stefszky, C. Vorvick, and D. Sigg, Opt. Express **21**, 19047 (2013).
37. Y. Takeno, M. Yukawa, H. Yonezawa, and A. Furusawa, Opt. Express **15**, 4321 (2007).
38. A. Schönbeck, F. Thies, and R. Schnabel, Opt. Lett. **43**, 110 (2018).